Electronic Supplementary Material (ESI) for ChemComm.
This journal is © The Royal Society of Chemistry 2020

Large Nonlinear Optical Effect in Tungsten Bronze Structures via Li/Na Cross-Substitutions

Shihang Chu,[a] Kun Lin,[a,*] Tao Yang,[a] Chenyi Yu,[a] Yili Cao,[a] Yujuan Zhang,[a] Yujiao Sun,[a] Zerui Li,[a] Xingxing Jiang,[b] Zheshuai Lin,[b] Qiang Li,[a] Jun Chen,[a] Kenichi Kato,[b] Hui Wu,[c] Qingzhen Huang,[c] Xianran Xing[a,*]

[a]*Beijing Advanced Innovation Center for Materials Genome Engineering, Institute of Solid State Chemistry, Department of Physical Chemistry, University of Science and Technology Beijing, Beijing 100083, China*

[b]*Technical Institute of Physics and Chemistry, Chinese Academy of Sciences, Beijing 100190, China*

[c]*Center for Neutron Research, National Institute of Standards and Technology, Gaithersburg, Maryland 20899-6102, United States*

1. EXPERIMENTAL SECTION

Polycrystalline samples were synthesized by solid state method using PbO, Na_2CO_3, Li_2CO_3 and Nb_2O_5 as raw materials with purities larger than 99.9%. Neutron powder diffraction were collected on the BT-1diffractometer at the Center for Neutron Research at the National Institute of Standards and Technology (USA) using a Cu monochromator (λ=1.5403Å) at room temperature (RT). High resolution X-ray diffraction (SPD) data at RT were collect at the 11-BM-B of the advanced photon source in Argonne National Laboratory with light wavelength of 0.41263 Å. High-temperature XRD were collected at the BL44B2 beamline of SPring-8 synchrotron radiation facility using a constant wavelength of 0.50026 Å.(*1*) The SHG measurement was conducted by Kurtz-Perry method using a pulsed Nd:YAG laser with an incident wavelength of 1064 nm.(*2*) Samples of both KH_2PO_4 and $LiNbO_3$ were used to reduce the uncertainty during the instrument setup. The polycrystalline samples were ground and sieved into distinct particle size ranges (~ 18 μm – 165 μm). Rotation electron diffraction (RED) data was collected on a JEOL JEM2100 TEM with very low dose electron beam by using the second condenser aperture. A single tilt sample holder with ±70° goniometer tilt was used. The TEM and camera were controlled by the RED program automatically and electron diffraction patterns were recorded by a Gatan ES500W Erlangshen camera.

2. CRYSTAL STRUCTURE DETERMINATION

According to previous studies, Pb-containing TTB niobates usually exhibit orthorhombic distorted structures with space group of C*m*2*m*, as reported in

$Pb_2KNb_5O_{15}$,(*3*) $Pb_xBa_{1-x}Nb_2O_6$ (x>0.7),(*4*) $Pb_{2(1-x)}K_{1+x}Gd_xNb_5O_{15}$ (x>0.35),(*5*) and $PbBiNb_5O_{15}$.(*6*) To reveal the crystal structures of the above two compounds, we fitted the SPD patterns using C*m*2*m* structural model firstly. However, there are a series of weak peaks cannot be indexed, as shown in Fig 1a. These may be caused by the superstructure reflections driven by the ordering of the crystal structures.

In order to further determine the accurate cell parameters and possible space groups, rotation electron diffraction (RED) experiments were carried out. The 3D reciprocal lattice was reconstructed from those ED frames and diffraction patterns along different directions are shown in Fig. 2d. In these figures, except for the strong main diffraction spots of the C*m*2*m* model, intermediate weak spots can be clearly observed, suggesting the existence of structural orderings with enlarged cells of ($2\sqrt{2}a_{TTB}$, $\sqrt{2}b_{TTB}$, $2c_{TTB}$). Considering the weak reflections, the existence of the systematic absences could be deduced from the 2D slices shown in Fig. 2a-c as 0*kl*: l=2n+1; h0l: h+l=2n+1 and hk0: h=2n+1, from which the possible space groups could be deduced to be noncentrosymmetric B22$_1$2 (No.20), Bb2$_1m$ (No.36), Bbm2 (No.40) and centrosymmetric Bmmb (No.63). Considering the measured strong SHG response and spontaneous volume ferroelectrostriction in these two compounds, centrosymmetric Bmmb and non-polar B22$_1$2 were excluded. Thus there are only two space groups (Bb2$_1m$ and Bbm2) with different polar directions worth considering (along $[110]_{TTB}$ for Bb2$_1m$ and along $[001]_{TTB}$ for Bbm2). The RED results of PLNN are consistent with the PN07N.

It has been known that the polar directions of TTB niobates are divided into two

types: along the stacking direction of the NbO_6 layer (the *c*-axis direction) or within the NbO_6 layer (the *a*-*b* plane). The latter case exists when certain Pb are in the A sites, such as $Pb_2KNb_5O_{15}$ and $PbNb_2O_6$.(*3,7*) In $Pb_{1-x}Ba_xNb_2O_6$ and $Pb_{2(1-x)}K_{1+x}Gd_xNb_5O_{15}$,(*4,5*) for example, the polar direction changes from the *b* axis to the *c* axis with reducing the Pb content. The case of PN07N and PLNN like those above. In addition, the spontaneous electric polarization in ferroelectrics usually induces an increase of the lattice along the polar axis, known as the spontaneous volume ferroelectrostriction (SVFS), which results in a negative thermal expansion (NTE) or weakened positive thermal expansion along this axis.[8] PN07N and PLNN exhibit a pronounced uniaxial NTE (-2.01×10^{-5} °C^{-1} in PN07N and -2.24×10^{-5} °C^{-1} in PLNN) exist along the polar *b* axis ($[110]_{TTB}$), indicating that PN07N and PLNN possess in plane (*a*-*b*) polarization and thus adopting the B*b*2_1*m* structure.

Following, the detailed crystal structures were verified and refined by high resolution neutron powder diffraction (NPD). Although both the C*m*2*m* and B*b*2_1*m* structural model could fit the SPD data well, a significant improved fitting by B*b*2_1*m* model happens in NPD (Fig. S3， Table S1).

3. CALCULATION DETAILS

The calculation was carried out using a structure model with 12.5% Pb + 25% Li + 50% Na + 15% □ (where □ represents a vacancy) in the quadrangle tunnels (from experiment results). The first-principles calculation based on plane-wave pseudopotential density functional theory (DFT) (*9*) was implemented by CASTEP

package (*10*).The local density approximation (LDA) method with the Ceperley and Alder, Perdew and Zunger (CA-PZ) functionals is adopted to describe the exchange and correlation (XC) term in the Hamiltonian The ultrasoft pseudopotentials (*11*) was used to describe the effective ion-electron interactions for all constituent elements. The kinetic energy cutoff 380 eV was chosen, and Monkhorst-Pack k-point meshes (*12*) spanning was set to less than 0.05 per $Å^{-3}$ in the Brillouin zone. Before the optical properties calculation, the cell parameters and atomic positions are geometry optimized using the quasi-Newton method (*13*). The convergence thresholds for energy, maximum force, maximum stress, and maximum displacement are set as 5×10^{-6} eV per atom, 0.01 eV per Å, 0.02 GPa and 5×10^{-4} Å, respectively. For energy bandgap E_g are usually underestimated by standard DFT theory, due to the discontinuity of the XC energy (*14*), the scissors-corrected LDA method is employed to calculate the optical properties, where the scissors operator is set as the difference between the experimental and calculated bandgaps. This approach has been used for the investigation of linear and nonlinear optical (NLO) properties in many types of NLO materials (*15*).

4. FIGURES AND TABLES

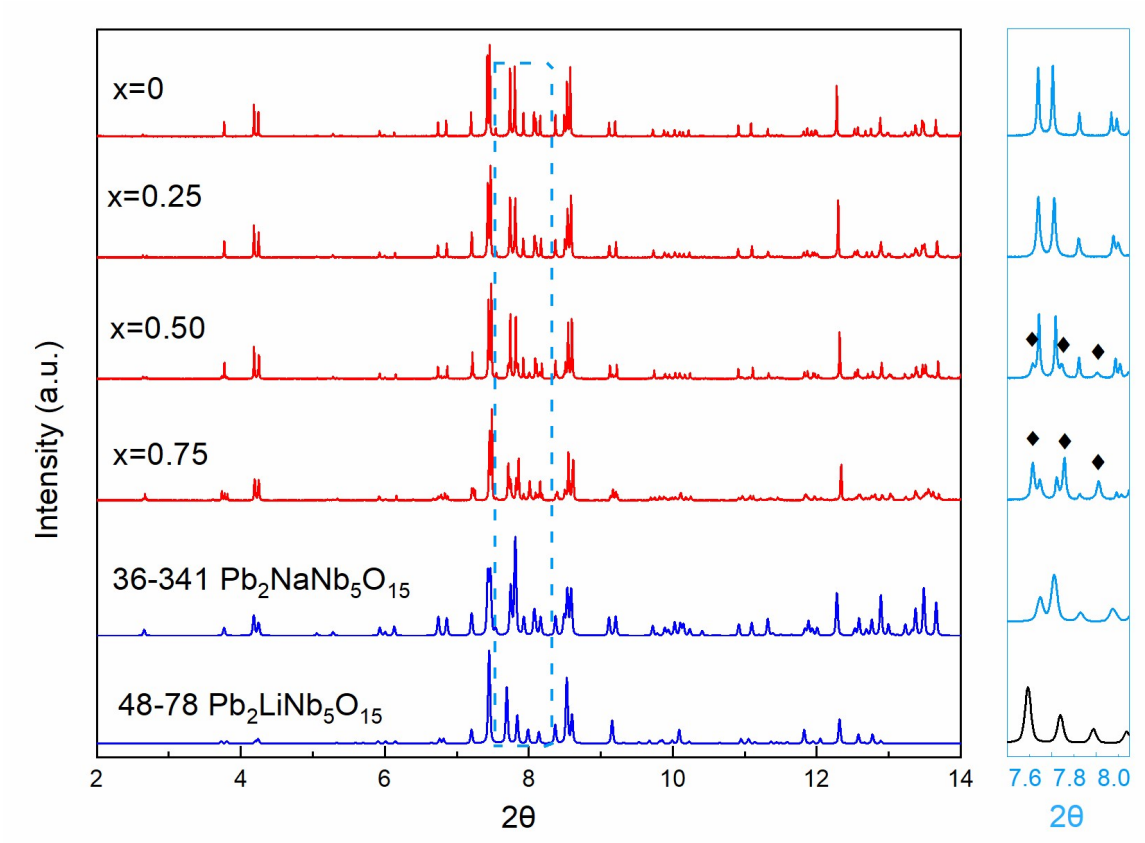

Fig. S1 The SPD patterns of $Pb_{2.15}(Li_xNa_{1-x})_{0.7}Nb_5O_{15}$ (x = 0, 0.25, 0.5, 0.75). (a) The whole patterns. (b) The part of XRD patterns for details (7.0°<2theta< 8.5°)

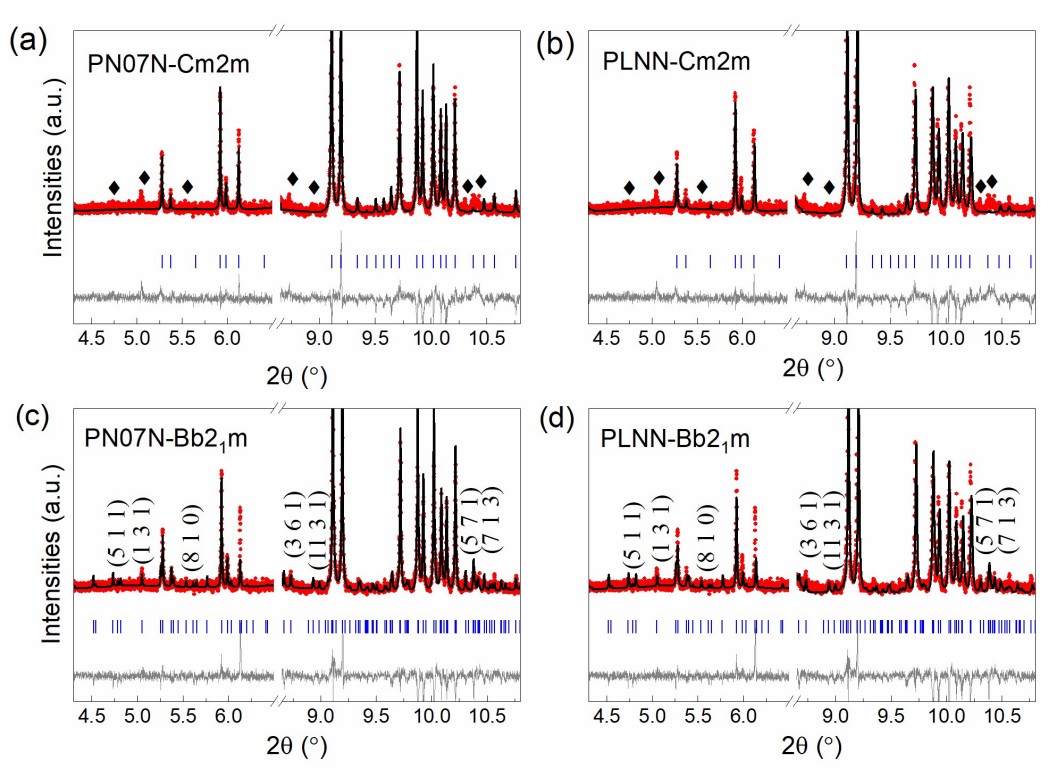

Fig. S2 Rietveld refinement patterns the RT SPD data for PN07N and PLNN using space groups C*m*2*m* (a,b) and Bb2$_1$m (c,d) in the range of $4 < 2\theta < 6°$and $8.5 < 2\theta < 11$. Observed (red scatter), calculated (black curve), Bragg reflections (blue bars) and difference (gray curves) are shown. Diamonds indicate the superstructure reflection that can not be indexed.

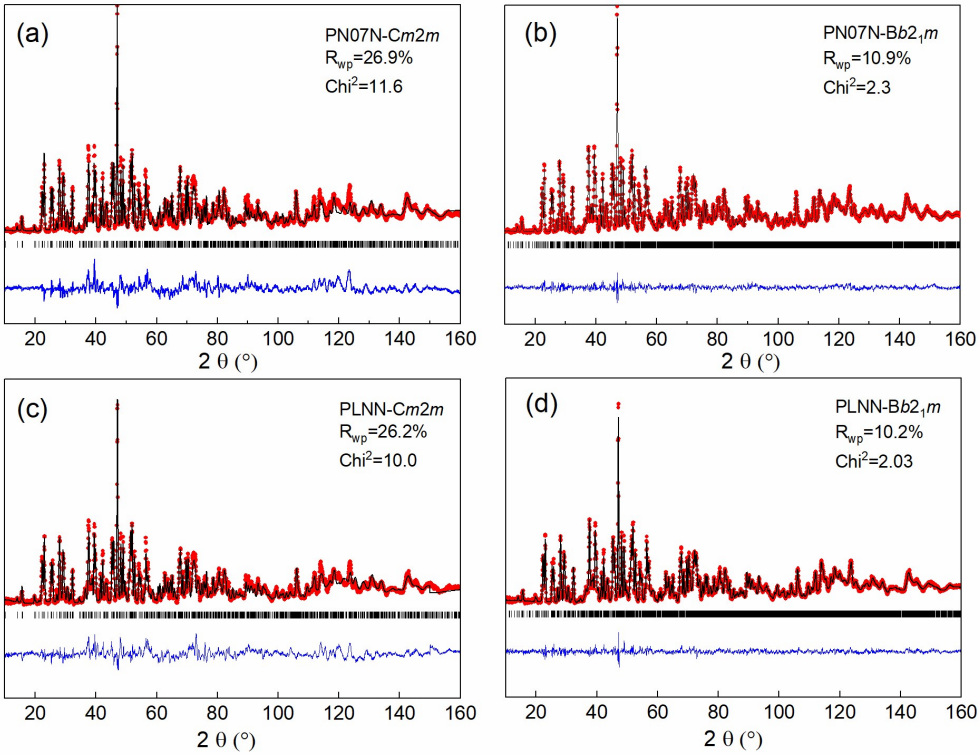

Fig. S3 Rietveld refinement patterns of NPD data for PN07N and PLNN using space group C*m*2*m* (a, c) and B*b*2_1*m* (b,d).

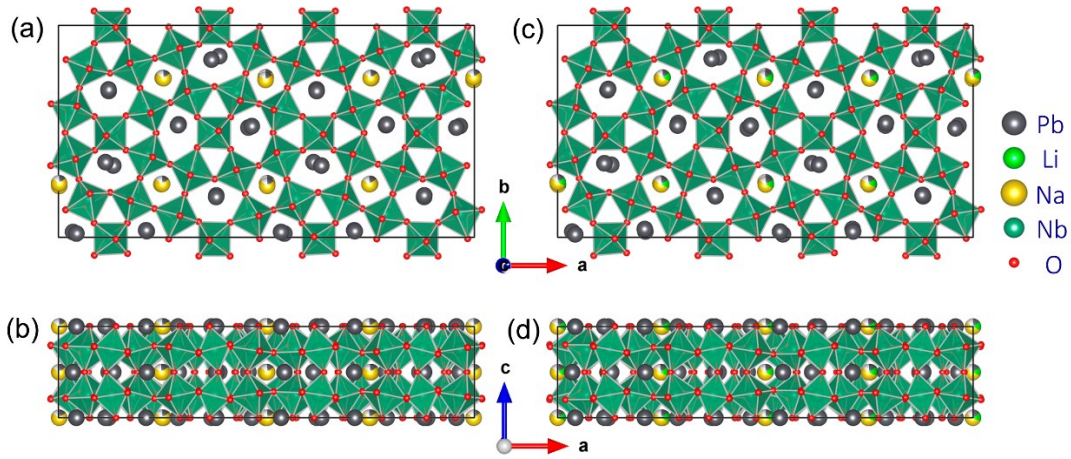

Fig. S4 Crystal structure of PN07N (a,b) and PLNN (c,d).

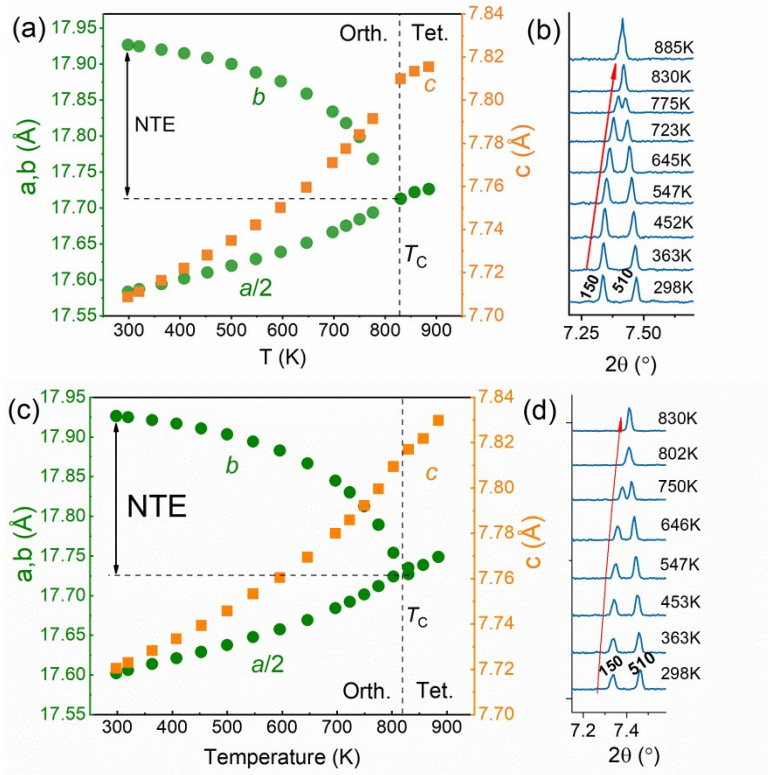

Fig. S5 (a,c) The evolution of unit cell parameters of PLNN (a) and PN07N (c) with temperature upon heating. (b,d) The shift of (150) and (510) reflections of PLNN (b) and PN07N (d) with temperature (indexed by C*m*2*m* model).

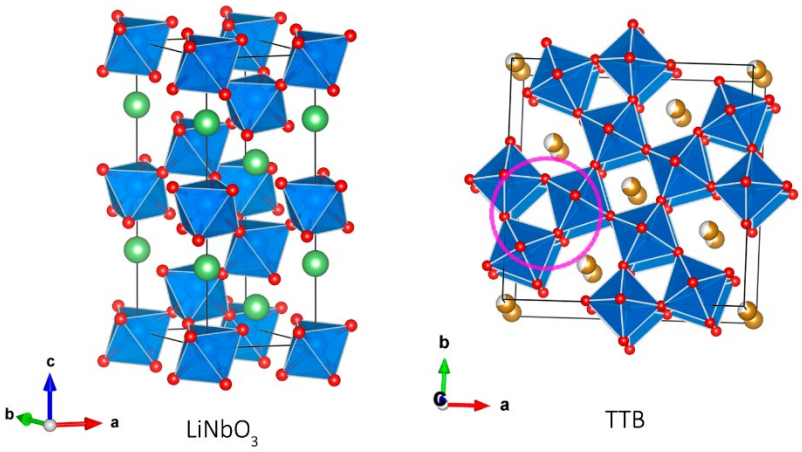

Fig. S6 The crystal structure of $LiNbO_3$ vs. TTB. The circle marks the triangle-like octahedra linkage in the TTB skeleton, which enables the structure to be stiffer.

Table S1 Crystallographic data for PN07N and PLNN

	PN07N	PLNN
Chemical formula	$Pb_{2.15}Na_{0.7}Nb_5O_{15}$	$Pb_{2.15}(Li_{0.25}Na_{0.75})_{0.7}Nb_5O_{15}$
Refinement method	Rietveld refinements	
Temperature	293(2)K	
Wavelength	1.5406Å	
Crystal system	Orthogonal	Orthogonal
Space group	B$b2_1m$	B$b2_1m$
Unit cell dimensions	a=35.206(0) Å	a=35.170(0) Å
	b=17.920(0) Å	b=17.923(0) Å
	c=7.721(1) Å	c=7.709(1) Å
	α=90(0)°	α=90(0)°
	β=90(0)°	β=90(0)°
	γ=90(0)°	γ=90(0)°
Volume (Å^3)	4871.56(1)	4859.80(1)
A-site occupancies	A1: 15%Pb, 70%Na	A1: 15%Pb, 52.5%Na, 17.5%Li
	A2: 100% Pb	A2: 100% Pb
Rietveld R-factors	R_p: 8.64%	R_p: 8.53%
	R_{wp}: 10.9%	R_{wp}: 10.2%
	R_{exp}: 7.03%	R_{exp}: 7.04%
	Chi^2: 2.30	Chi^2: 2.03

Table S2 The SHG intensities of related TTB compounds using both KDP and $LiNbO_3$ as the reference.

Codes	Compounds	SHG intensities
KDP	KH_2PO_4	0.0271±0.001
LN	$LiNbO_3$	1.069±0.03
PLN	$Pb_{2.15}Li_{0.7}Nb_5O_{15}$	1.143+0.04
PN07N	$Pb_{2.15}Na_{0.7}Nb_5O_{15}$	0.879±0.04
PLNN	$Pb_{2.15}(Li_{0.25}Na_{0.75})_{0.7}Nb_5O_{15}$	1.377±0.11

Table S3 The calculated values of second-order nonlinear coefficients for PLNN.

	d_{15}	d_{24}	d_{33}
All	2.5	-4.92	9.57
Li	0.02	-0.06	0.06
Na	0.09	0.08	0.21
Nb-O	2.96	-5.48	11.98
Pb-O	0.63	-0.78	2.22

5. REFERENCES

1 Kato, K., Tanaka, Y., Yamauchi, M., Ohara, K. & Hatsui, T. A statistical approach to correct X-ray response non-uniformity in microstrip detectors for high-accuracy and high-resolution total-scattering measurements. *J. Synchrotron Rad.* **26**, 762-773 (2019).

2 Kurtz, S.K. A Powder Technique for the Evaluation of Nonlinear Optical Materials. *J. Appl. Phys.* **39**, 3798-3813 (1968).

3 Lin, K. *et al.* Structure and thermal expansion of the tungsten bronze $Pb_2KNb_5O_{15}$. *Dalton.*

Trans. **43**, 7037-7043 (2014).

4 Venet, M., Zabotto, F.L., Eiras, J.A. & Garcia, D. Improvement of the phase diagram for the pseudobinary $PbNb_2O_6$–$BaNb_2O_6$ system. *J. Appl. Phys.* **105**, 124106 (2009).

5 Amira, Y. *et al.* Structural and Raman properties of the tetragonal tungsten bronze ferroelectric$Pb_{2-x}K_{1-x}Gd_xNb_5O_{15}$. *Solid State Commun.* **150**, 419-423 (2010).

6 Lin, K. *et al.* Unusual Strong Incommensurate Modulation in a Tungsten-Bronze-Type Relaxor $PbBiNb_5O_{15}$. *J. Am. Chem. Soc.* **137**, 13468-13471 (2015).

7 Labbé, P., Frey, M., Raveau, B. & Monier, J.C. Structure cristalline de la phase ferroélectrique du niobate de plomb $PbNb_2O_6$. Déplacements des atomes métalliques et interprétation de la surstructure. *Acta Cryst. B* **33**, 2201-2212 (1977).

8 (a) Chen, J., Hu, L., Deng, J. & Xing, X. Negative thermal expansion in functional materials: controllable thermal expansion by chemical modifications. *Chem. Soc. Rev.* **44**, 3522-67 (2015). (b) Chen, J. *et al.* Effectively control negative thermal expansion of single-phase ferroelectrics of $PbTiO_3$-(Bi,La)FeO_3 over a giant range. *Sci. Rep.* **3**, 2458 (2013).

9. W. Kohn, L.J. Sham, Self-Consistent Equations Including Exchange and Correlation Effects. *Phys. Rev.* **140**, 1133-1138 (1965).

10. S.J. Clark, M. D. Segall, *Z. Kristallogr.* 2005, 220, 567-570.

11. D. Vanderbilt, Soft self-consistent pseudopotentials in a generalized eigenvalue formalism. *Phys. Rev. B* **41**, 7892-7895 (1990).

12. H.J. Monkhorst, J.D. Pack, Special points for Brillouin-zone integrations. *Phys. Rev. B* **13**, 5188-5192 (1976).

13. B. G. Pfrommer, M. Côté, S. G. Louie, M. L. Cohen, Relaxation of crystals with the quasi-newton method. . *Comp. Phys.***131**, 233-240 (1997).

14. C.S. Wang, B.M. Klein, First-principles electronic structure of Si, Ge, GaP, GaAs, ZnS, and ZnSe. II. Optical properties. *Phys. Rev. B* **24**, 3417-3429 (1981).

15. Z.S. Lin, *et al.,* First-principles materials applications and design of nonlinear optical crystals. *J. Phys. D: Appl. Phys.* **47**, 253001-253019 (2014).